Hindawi
Advances in Materials Science and Engineering
Volume 2019, Article ID 8053248, 11 pages
https://doi.org/10.1155/2019/8053248

Research Article

Fatigue Life Behavior of Laser Shock Peened Duplex Stainless Steel with Different Samples Geometry

César A. Vázquez Jiménez,[1] **Vignaud Granados Alejo**,[2,3] **Carlos Rubio González**,[2] **Gilberto Gómez Rosas**,[4] **and Sergio Llamas Zamorano**[1]

[1]*Facultad de Ingeniería Mecánica y Eléctrica, Delegación 4, Universidad de Colima, Coquimatlán, Colima 28400, Mexico*
[2]*Centro de Ingeniería y Desarrollo Industrial, Pie de la cuesta 702, Desarrollo San Pablo, Querétaro, Qro. 76130, Mexico*
[3]*Universidad Politécnica de Guanajuato, Universidad Sur 1001, Juan Alonso, Cortazar, Gto. 38496, Mexico*
[4]*Departamento de Física, Centro Universitario de Ciencias Exactas e Ingenierías, Universidad de Guadalajara, Guadalajara, Jalisco 44430, Mexico*

Correspondence should be addressed to César A. Vázquez Jiménez; vazquez_cesar@ucol.mx

Received 25 June 2019; Accepted 31 August 2019; Published 31 October 2019

Guest Editor: Alexander Balitskii

Two different stress raiser geometries (fillets and notched) were treated by laser shock peening (LSP) in order to analyze the effect of sample geometry on fatigue behavior of 2205 duplex stainless steel (DSS). The LSP treatment was carried through Nd : YAG pulsed laser with 1064 nm wavelength, 10 Hz frequency, and 0.85 J/pulse. Experimental and MEF simulation results of residual stress distribution after LSP were assessed by hole drilling method and ABAQUS/EXPLICIT software, respectively. The fatigue tests (tensile-tensile axial stress) were realized with stress ratio of $R = 0.1$ and 20 Hz. A good comparison of residual stress simulation and experimental data was observed. The results reveal that the fatigue life is increased by LSP treatment in the notched samples, while it decreases in the fillet samples. This is related to the residual stress distribution after LSP that is generated in each geometry type. In addition, the fatigue crack growth direction is changed according to geometry type. Both the propagation direction of fatigue crack and the anisotropy of this steel results detrimental in fillet samples, decreasing the number of cycles to the fatigue crack initiation. It is demonstrated that the LSP effect on fatigue performance is influenced by the specimen geometry.

1. Introduction

Through surfaces engineering, it is possible to improve the surface properties of materials without changing the bulk material. Different surface treatments, such as shot peening, cavitation peening, laser shock peening, ultrasonic peening, deep rolling, among others, have proven to be effective techniques to increase the service time of mechanical elements. In recent years, the LSP treatment has been focused on fatigue behavior in different metal alloys due to its effectiveness in improving their mechanical properties [1]. During the first stage of the fatigue process, when applying an external load, the yield stress in localized regions (crystalline defects) is exceeded. The plastic deformation continues accumulating as more load cycles take place until one or more cracks are incubated. By inducing residual compression stresses through the LSP treatment and taking into account the superposition principle, in order to exceed the yield stress in these localized regions, it is necessary that the external load first counteract the compression state induced in the material and, subsequently, begins to deform in a tension state. In this way, the LSP treatment decreases the effect of the applied external load and delays the incubation time of the cracks.

Several investigations have been carried out around different LSP parameters in order to optimize the LSP process on fatigue response of different metal alloys. Rubiogonzalez et al. founded that as the density of pulses increases, the fatigue crack growth rate decreases in compact tension samples of Al-6061-T6 [2] and 2205 DSS [3]. The fatigue life behavior as function of laser swept direction was optimized for bending fatigue in Ti-6Al-2Sn-4Zr-2Mo [4]

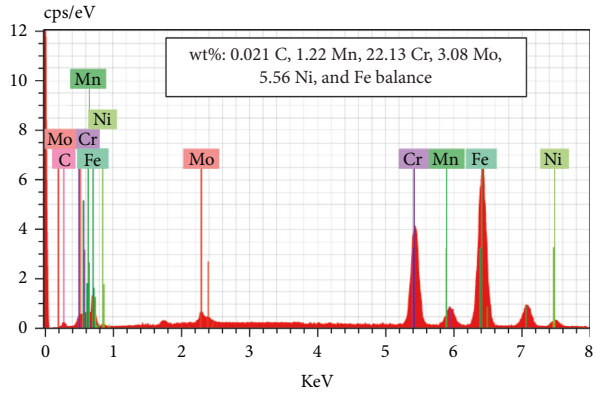

Figure 1: Chemical composition of 2205 cold rolled plate.

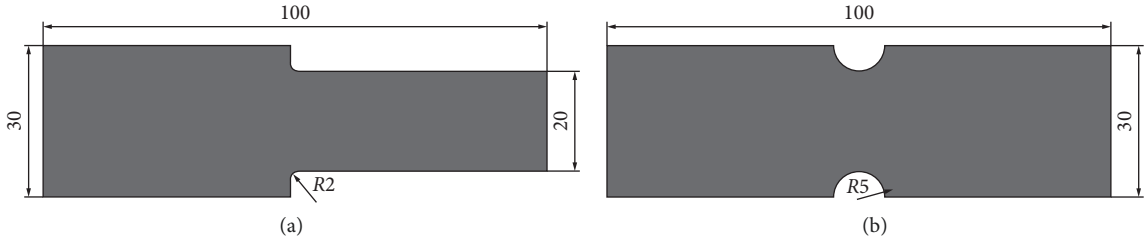

Figure 2: Specimens dimensions for fatigue tests (mm): (a) fillet and (b) notched.

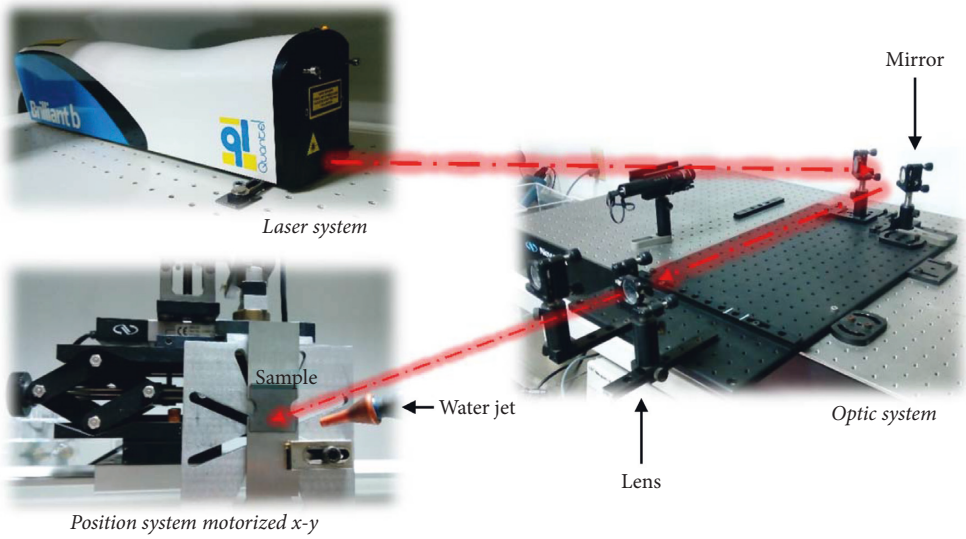

Figure 3: Experimental arrangement of LSP.

and tensile-tensile fatigue test to 2024-T351 [5], 2205 DSS [6], and 316L [7] alloys. Different fatigue behaviors were observed varying the swept direction for each case, demonstrating a high influence of this LSP parameter on fatigue life behaviors of these alloys. Sheng et al. [8] and Huang et al. [9] analyzed the morphology of fracture surface and the fatigue crack growth rate of 6061-T6. It is founded that as the laser pulse energy increases, both the fatigue striation spacing and fatigue crack growth rate decrease. The fatigue response as a function of coverage area paths was analyzed by Huang et al. in Ti-6Al-4V [10] and 6061-T6 [11] alloys. It is demonstrated the fatigue properties are influenced directly by this LSP parameter decreasing the fatigue crack growth rate in both materials.

On the other hand, for other test conditions such as specimens submitted to high temperature during fatigue test [12, 13] and specimens with previous damage (pre-fatigued) [14, 15], the LSP also has been an effective technique to improve the fatigue properties. Further, the effects on chemical composition after LSP and geometric

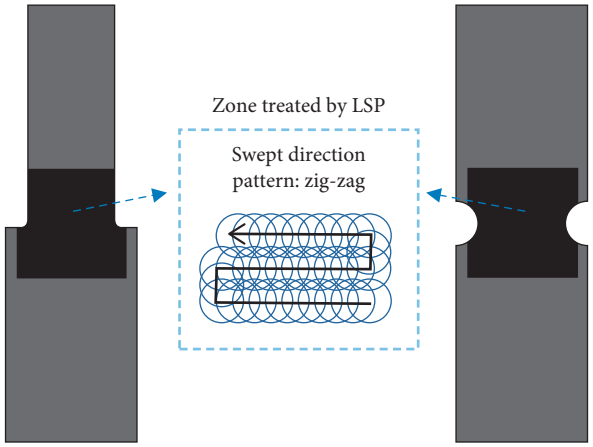

Figure 4: LSP Pulse sequence.

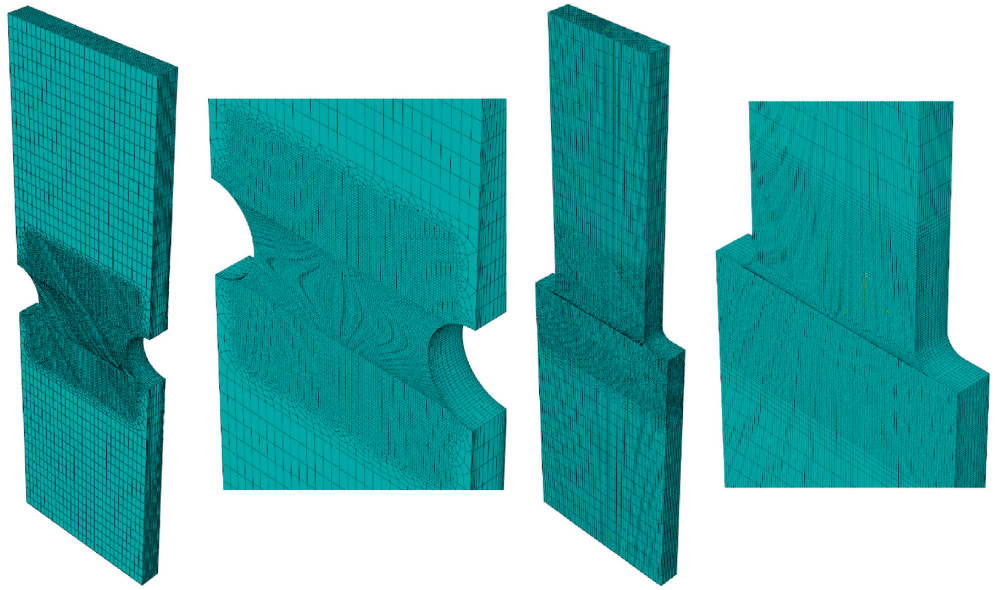

Figure 5: Finite element model of (a) notched and (b) fillet samples.

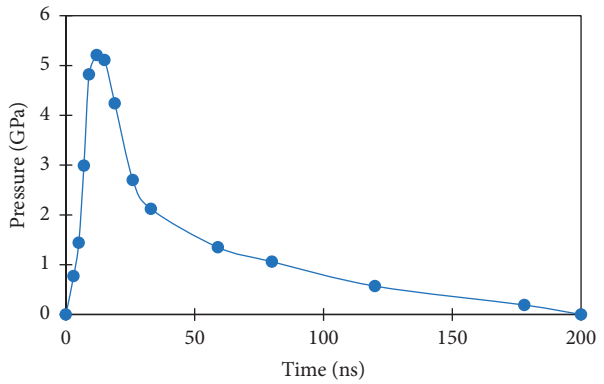

Figure 6: Plasma pressure profile.

Table 1: Johnson-Cook parameters for DSS 2205.

A (MPa)	B (MPa)	C	n	m	$\dot{\varepsilon}_0$
520	840.50	0.0124	0.1904	0.965	1

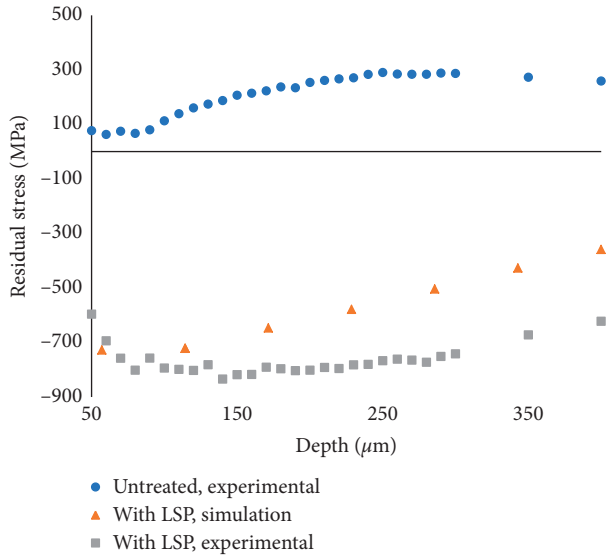

Figure 7: Experimental and simulation comparison of residual stress distribution.

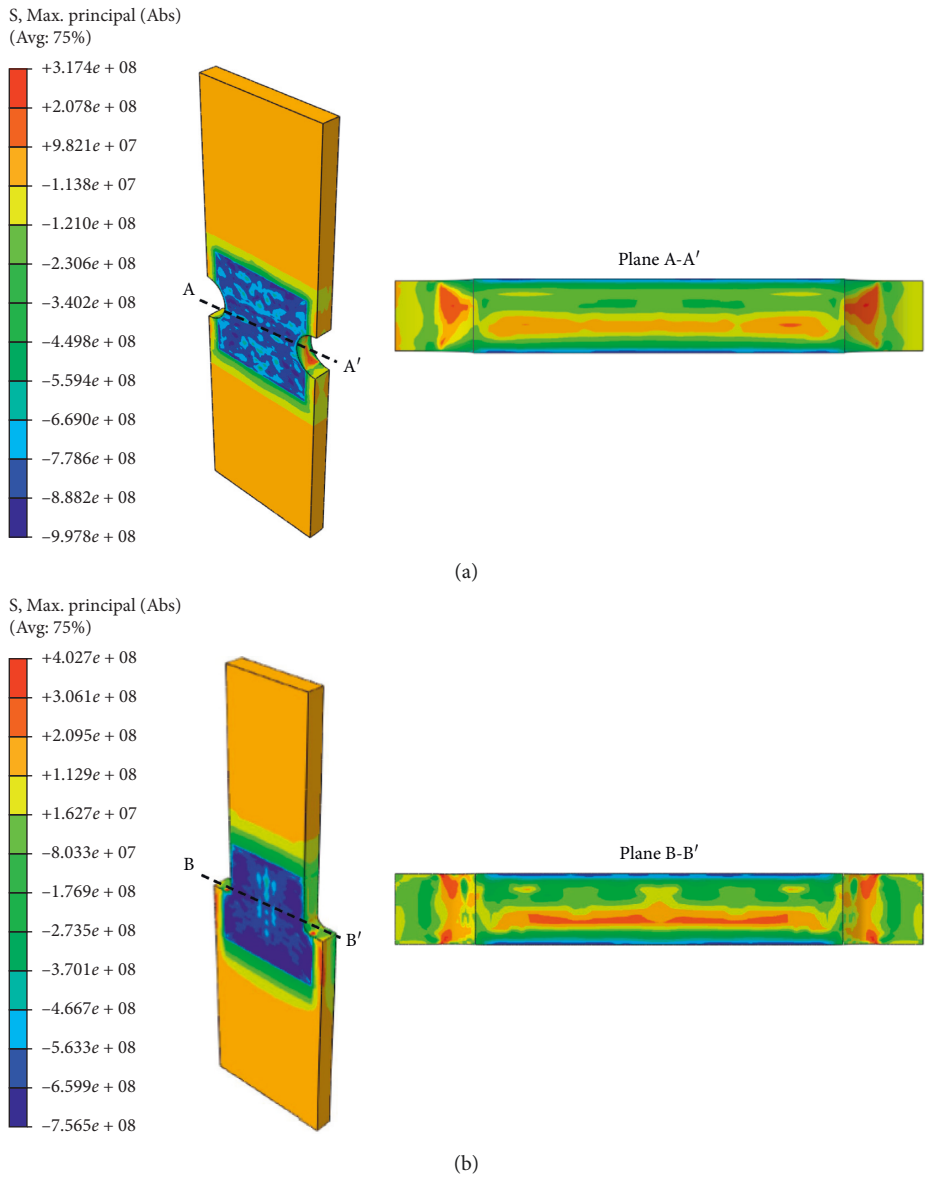

Figure 8: Results of MEF simulation: (a) Residual stress distribution after LSP in notched sample and (b) Residual stress distribution after LSP in filled sample.

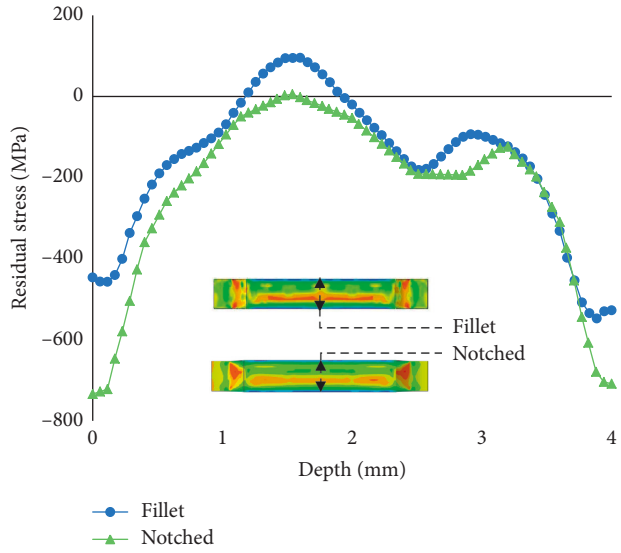

Figure 9: MEF simulation results of residual stress distribution in depth at midpoint of width.

factors, such as thickness and stress raisers, also have great influence on fatigue behavior. Rubio-gonzalez et al. [16] demonstrated that the LSP treatment in addition to the other treatment (Cold expansion) improves the fatigue life in open-hole samples of 6061-T6 Al alloy. However, individually, the LSP treatment resulted to have a detrimental effect on the fatigue crack initiation stage and a beneficial effect on the fatigue crack growth stage. Spadaro et al. [17] analyzed the effect of pulse density on low cycle fatigue in super-ferritic stainless steel and it is observed that the LSP causes thermal effects on the surface microstructure, generating intergranular corrosion, which decreases the fatigue life of this alloy. Bergant et al. [18] founded that the LSP increases fatigue crack growth rate in 6082-T651 Al alloy due the equilibrium tensile stresses in the center of specimen and notches edge as explained by Correa et al. [5, 7] through MEF simulation. Granados-Alejo et al. [19] analyzed the effect of samples thickness in 2205 DSS, in which it is observed that in thinner samples, higher fatigue life is obtained by LSP. This behavior is explained through the equivalent plastic strain distribution variations associated with the change in thickness of LSP treated samples. Similar trend about the sample thickness effects in 2024 Al alloy was observed by Achintha et al. [20]. For thick samples (~15 mm), the LSP had no effect on the fatigue life of this alloy. While for thin samples (~5 mm), the fatigue life was improved. The operation sequence of LSP without coating [21] and with coating [22] was investigated in thin open-hole samples for 6082-T6 and LY12CZ Al alloys, respectively. Similar observations are realized in both works, and higher fatigue life was observed in samples with hole drilled after LSP than samples with hole drilled before LSP. This phenomenon is related to residual stress distribution that was assessed by MEF simulation of LSP process.

It is known that other factors unrelated to LSP treatment parameters such as sample geometry, operation sequence and chemical composition, among others, are extremely sensitive to fatigue behavior of different metal alloys. In additions, no previous work has been reported the effect of LSP on fatigue behavior of fillet samples. In this work, two different geometries are compared (notches and fillets) taking into account the same operation sequence and LSP conditions in order to analyze the influence of sample geometry on fatigue life behavior of 2205 DSS. Additionally, the finite element simulation of the LSP process on notched and fillets samples are presented. The residual stress distribution was performed using the commercial code ABAQUS/Explicit and hole drilling method. In addition, the fracture surface is analyzed by SEM microscopy.

2. Material and Methods

The chemical composition results (in weight percentage) and the spectrum obtained through the EDS analysis are shown in the Figure 1. The mechanical properties were investigated by conducting the tensile test according to ASTM E24-08. The ultimate tensile strength, yield strength, elastic modulus, and elongation are 710 MPa, 520 MPa, 190 GPa, and 50%, respectively. Cold rolled plate of 9.5 mm thickness was machined to 4 mm (samples thickness). Special care was taken to cut the samples with a high-pressure water jet to reduce thermal damage on stress raiser geometries. The sample dimensions used in this work are displayed in Figure 2. The specimens were machined with the rolling axis parallel to the longitudinal axis. As reference, both 5 mm and 2 mm radius were selected with a similar stress concentration factor ($K_t = 2$) for the notched and fillet samples, respectively.

The laser technology system implemented to perform the treatments is shown in Figure 3 and consists of a Nd : YAG pulsed laser source with a wavelength of 1064 nm and a frequency of 10 Hz. During LSP, the laser beam (0.85 J, 6 ns) is directed and focused to 1 mm (spot diameter) on the sample surface through an optical system. The sample is moved with a position control device to generate the pulse sequence (zig-zag pattern) as shown in Figure 4. The pulses density and treated area were 2500 pulses/cm^2 and

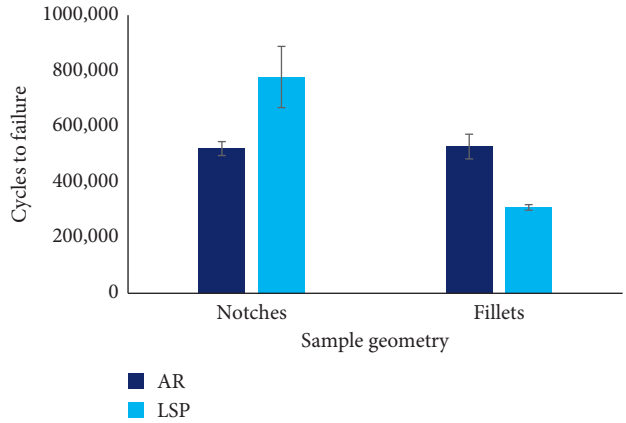

Figure 10: Fatigue life for different sample geometry in function of samples geometry for treated and untreated samples.

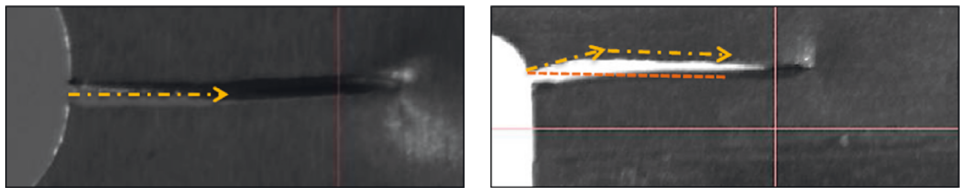

(a) (b)

Figure 11: Fatigue crack growth direction of (a) notches; (b) fillets.

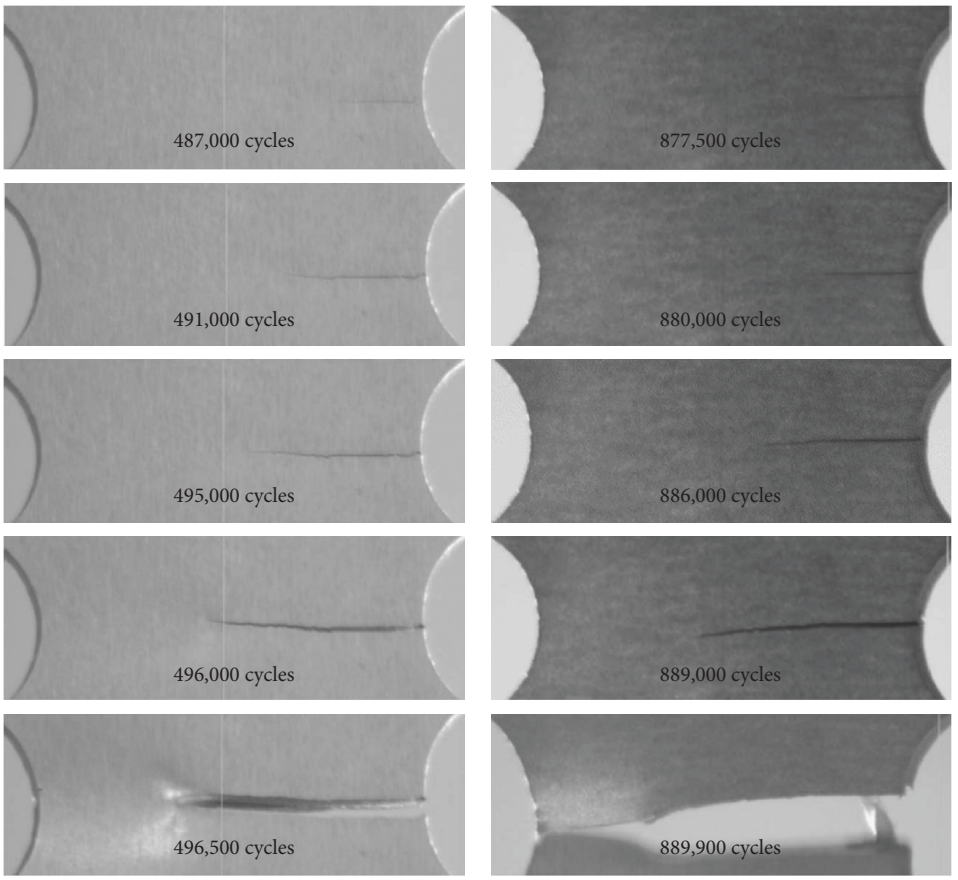

(a) (b)

Figure 12: Fatigue crack growth evolution in notched samples: (a) AR; (b) LSP.

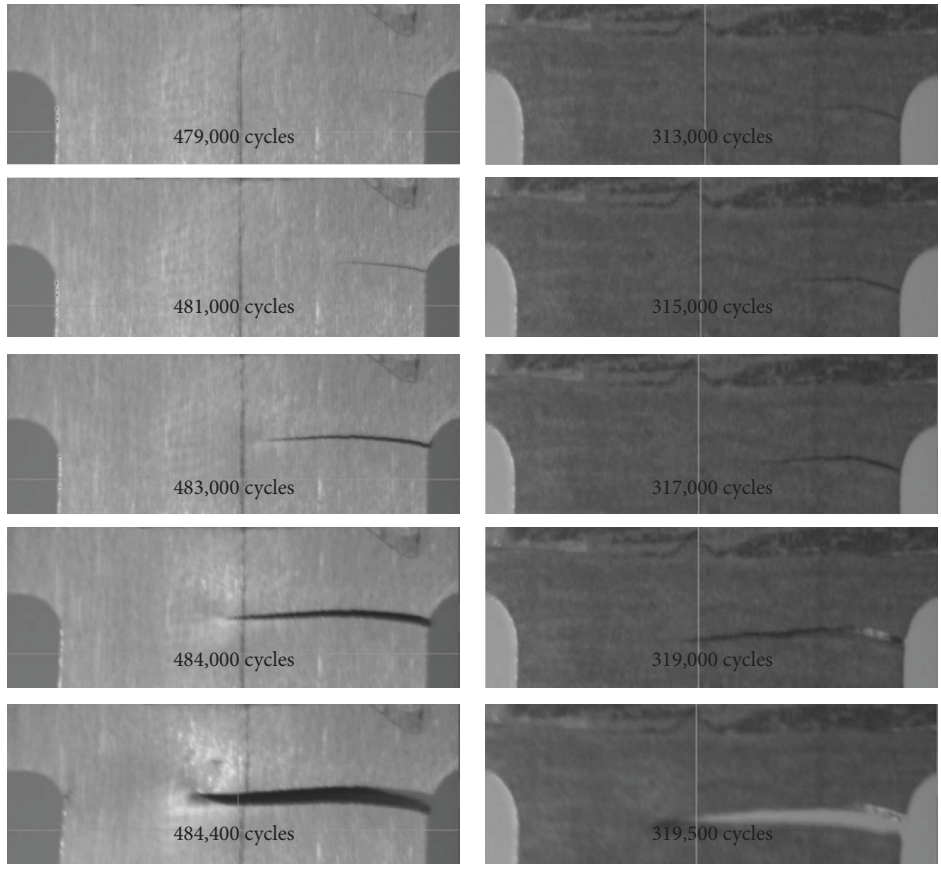

Figure 13: Fatigue crack growth evolution in fillet samples: (a) AR; (b) LSP.

$25 \times 25\,\text{mm}^2$, respectively, in both sides of the samples. A water jet device was used to form thin layer water on samples surface during the LSP treatments. The samples without LSP treatment will be hereinafter called as-received (AR).

Tensile-tensile fatigue test was carried out with MTS-810 servo-hydraulic machine with a load ratio of $R = 0.1$ and a frequency of 20 Hz. The experiments were realized at room temperature in the air. The loading applied on all the specimens was 24 kN, corresponding to maximum applied stress in reduced area of 300 MPa. The fatigue crack growth was monitored by a high-speed CCD camera using a magnification of 10x and the residual stress measurements were realized according to ASTM E28-04 by hole drilling method.

2.1. MEF Simulation. The commercial code ABAQUS/Explicit was used to estimate the residual stress distribution. The transient response of the laser pulse and the subsequent relaxation of the stress state constitute the numerical analysis. The FE model is shown in Figure 5. 190,512 C3D8R linear hexahedron elements were used for fillet sample and 224,826 for notched sample.

The pressure pulse was applied on 25×25 mm square. The time evolution is presented in Figure 6. Peak pressure of 5.21 GPa was obtained according to [23]. The LSP simulation process was simplified to one big laser shot according to [19].

The material model used to simulate the behavior of the material under the shock conditions (equation (1)) was the Johnson-Cook model,

$$\sigma = \left(A + B\varepsilon_{\text{eq}}^{n}\right)\left[1 + C\ln\left(\frac{\dot{\varepsilon}}{\dot{\varepsilon}_0}\right)\right]\left[1 - \left(\frac{T - T_0}{T_m - T_0}\right)^{m}\right], \quad (1)$$

with material constants are given in Table 1 [19].

3. Results and Discussion

3.1. Residual Stress Distribution. The comparison of the experimental and simulation results of the residual stresses distribution is shown in Figure 7. Compressive residual stresses are induced after LSP. The MEF simulation results show a similar trend to the experimental data. Figure 8 shows MEF simulation of residual stress distribution in the cross-section for notched (Figure 8(a)) and fillet (Figure 8(b)) samples.

It is observed that the LSP generates different residual stress distribution in each geometry type. The LSP treatment induces compressive residual stresses near surface. However, the balance of stress state generate tensile residual stresses at middle section of the thickness. The fillet sample present high

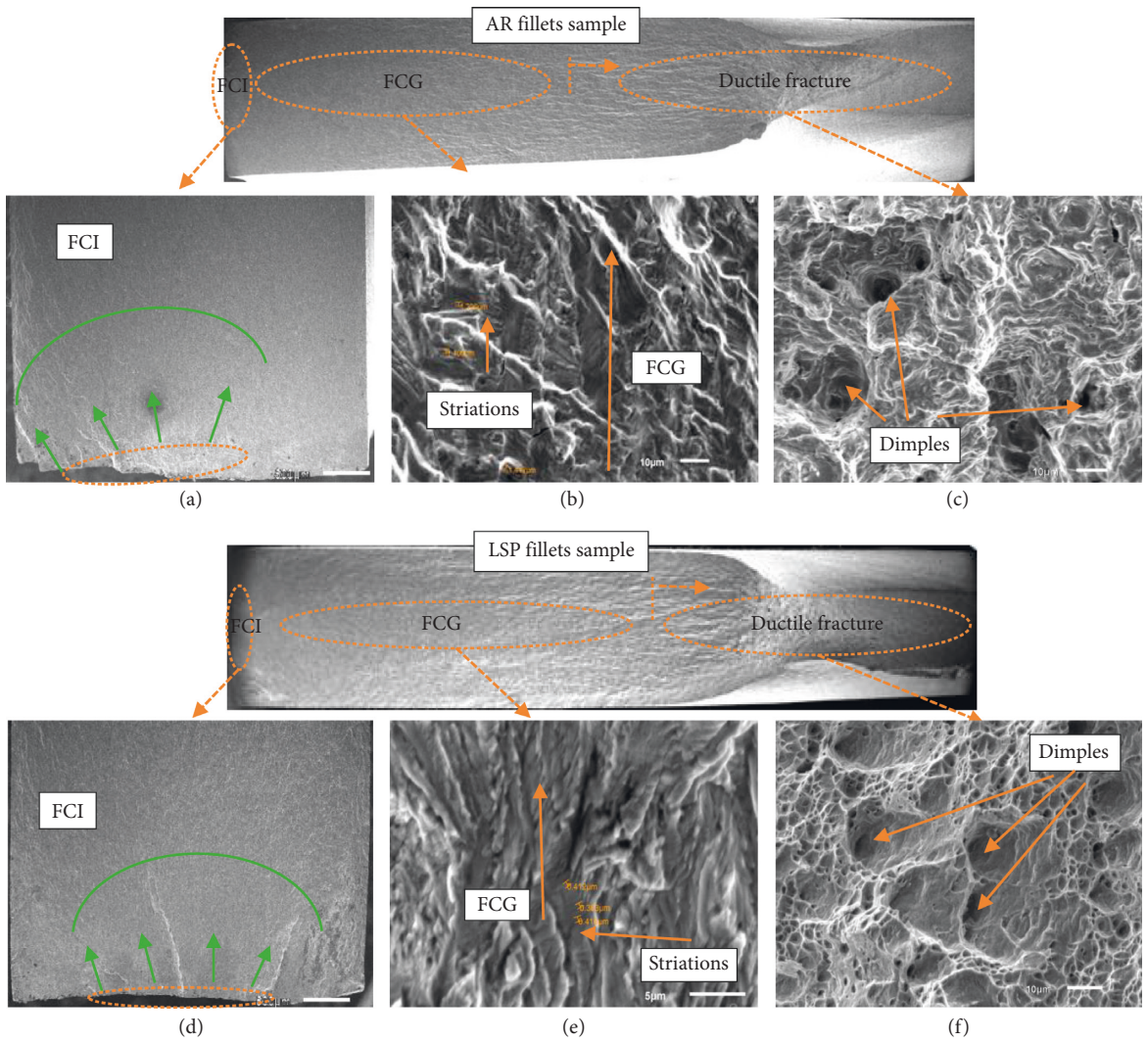

Figure 14: Fracture surfaces of the specimens with filet: (a, d) crack initiation, (b, e) fatigue crack growth, and (c, f) final rupture.

levels of tensile residual stresses near middle section of thickness in comparison of the notched sample. The residual stress profile in depth at midpoint of width is shown in Figure 9. In this point, the fillet sample presents a maximum value of tensile residual stress of 95.0 MPa at 1.6 mm depth. While the notched sample presents 5.3 MPa at 1.54 mm depth, a significant difference of 89.7 MPa between notched and fillet samples was observed. The constant area reduction of fillet sample could modify the residual stress distribution. The notched geometry has a symmetric axis in cross-direction that distributes the residual stress field more evenly in comparison with asymmetric axis corresponding to fillet sample. Several works have demonstrated that both the pulse sequence [24, 25] and the coverage area [26] modify the distribution of residual stress in sample edge and the middle of thickness. Further, other geometrical parameters such as the sample thickness also have a significant effect on the distribution of residual stresses as reported in [19, 27]. In this work, the same treatment condition was used in both sample geometries. It is evident that the geometry type is also an important factor which influences the residual stress distribution.

3.2. Fatigue Test. Fatigue test results are shown in Figure 10. It is observed that in notched samples, the LSP increases the number of cycles to failure of 521,500 for AR samples and to 779,450 after LSP. While in fillet samples, the LSP decreases the number of cycles to failure of 528,900 for AR samples and to 309,500 after LSP. It is observed that the LSP has different effects on fatigue behavior according to the sample geometry type tested, improving only the fatigue properties in notched samples. It is correlated with residual stress results in notched samples that showed higher compressive residual stress near surface and less tensile residual stress at middle of the sample thickness in comparison with fillet samples. Figure 11 shows the fatigue crack growth direction for each geometry type. The notched samples present a symmetric horizontal axis (perpendicular to loading axis) and the fatigue crack growth direction is given in this direction as shown in Figure 11(a). From Figure 11(b), it is observed that the fillet samples present an asymmetric horizontal axis and it has changed the fatigue short crack growth direction to an inclined plane and then return to the horizontal direction perpendicular to axis loading. It is

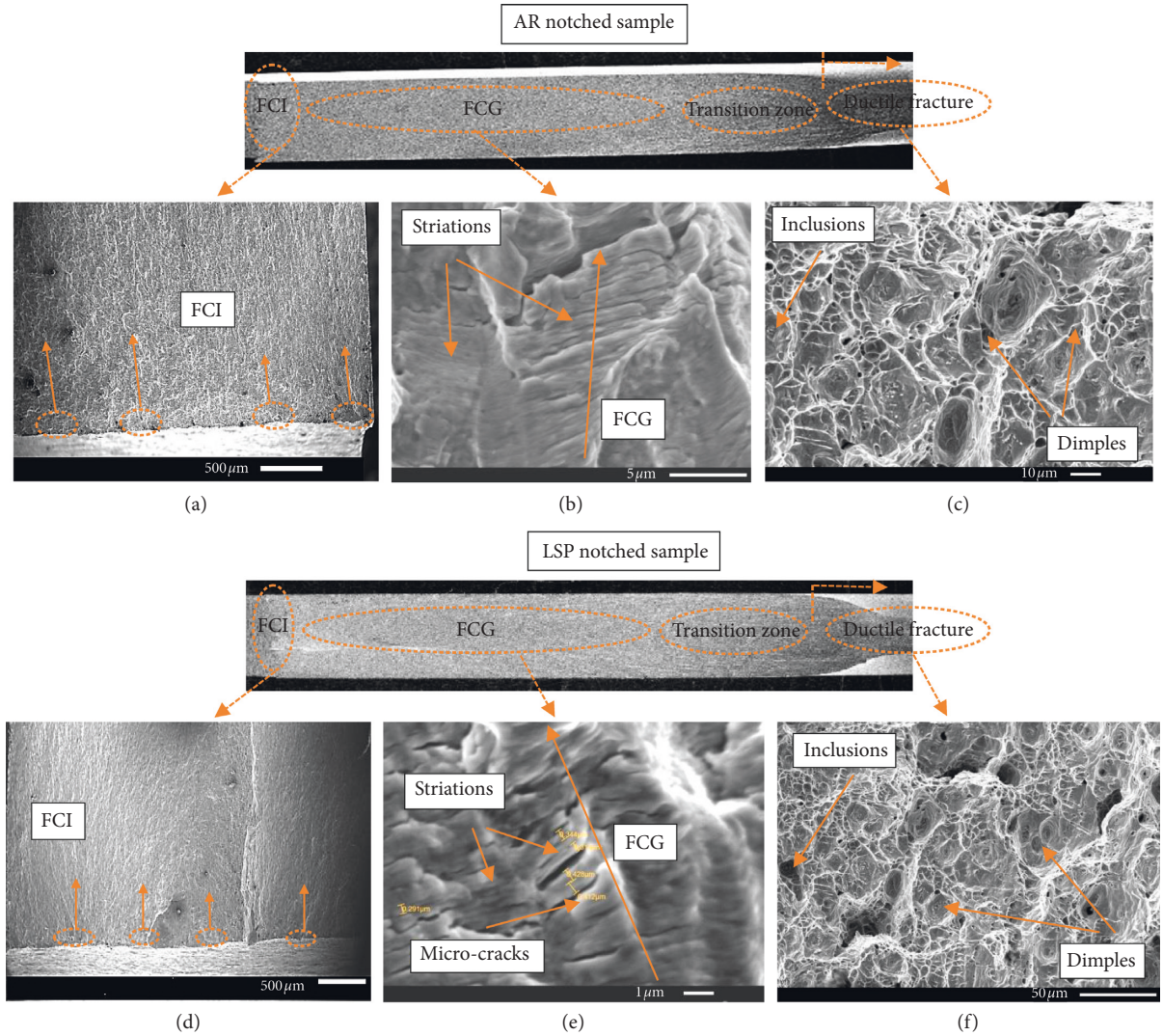

Figure 15: Fracture surfaces of the 4 mm thick specimen: (a, d) crack initiation, (b, e) fatigue striation, and (c, f) final rupture. Figure 15 is reproduced from Granados-Alejo et al. [19].

evident that the geometry type changes the preferential direction of fatigue crack growth. According to anisotropic effects reported in [28, 29], this direction change could influence fatigue results in fillet samples.

The fatigue crack evolution in treated and untreated notched samples is shown in Figure 12. For untreated samples (Figure 12(a)), the fatigue crack appears at surface at 487,000cycles and then 9,500 cycles elapse, accumulating 496,500 cycles to failure. While in treated samples (Figure 12(b)), the fatigue crack appears at surface at 877,500 cycles and then 12,400 cycles elapse, accumulating 889,900 to failure. It is observed that the LSP improves both the fatigue crack initiation and growth in notched samples.

The fatigue crack evolution in treated and untreated fillet samples is shown in Figure 13. For untreated samples (Figure 13(a)), the fatigue crack appears at the surface at 479,000 cycles and then 5,400 cycles elapse, accumulating 484,400 cycles to failure. While in treated samples (Figure 13(b)), the fatigue crack appears at surface at 313,000 cycles and then 6,500 cycles elapse, accumulating 319,500 to failure. It is observed that the LSP improves the fatigue crack growth stage while it is detrimental for the fatigue crack initiation stage in fillet samples. It is well known that the fatigue crack initiation depends on microstructural parameters such as crystallographic orientation, grain size, phase distribution, and the interaction of elastic and plastic properties between the austenite and ferrite phases [28, 30, 31]. In this stage, the short crack is propagating in the plane of the maximal shear stress. In the fatigue crack growth stage, the microstructural effects are inhibited, and the fatigue crack grows perpendicular to loading axis. In this stage, the compressive residual stress induced by LSP decreases stress ratio R according to superposition principle [32] and consequently the fatigue crack growth rate (da/dN) decreased.

3.3. Fracture Surface. The fracture surface for notched and fillet samples is shown in Figures 14 and 15, respectively. The LSP effect changes the fatigue crack initiation zone in

both samples' geometries from the border in AR samples (Figures 14(a) and 15(a)) at mid-thickness in treated samples (Figures 14(d) and 15(d)). The LSP induces high level of compressive residual stresses and hardening layer [33] that improves the surface properties causing this shift. Details of stable crack growth zone are shown in Figures 14(b) and 15(b) for untreated samples and Figures 14(e) and 15(e) for treated samples. The average value of fatigue striation spacing in AR samples is 0.748 and 1.337 μm for notched and fillet samples, respectively. While in treated samples, the average value of fatigue striation spacing is 0.346 and 0.403 μm for notched and fillet samples, respectively. In both cases, a lower value of fatigue striation spacing after LSP was observed, indicating a decrease in fatigue crack growth rate according to experimental results of fatigue tests. The final fracture is shown in Figures 14(c) and 15(c) for untreated samples and Figures 14(f) and 15(f) for treated samples. In both cases, similar mechanism of ductile failure is observed.

4. Conclusions

The influence of LSP on fatigue life of 2205 DSS with different sample geometry has been investigated. The LSP improves the surface properties of 2205 DSS increasing the fatigue life on notched samples. However, the fillet samples modify the residual stress distribution and change the short fatigue crack growth inhibiting the LSP effect.

The numerical simulation of residual stress distribution was used as powerful tools to predict and correlate this result with the fatigue behavior of the 2205 DSS. A good approximation between experimental and simulation results was obtained.

Both the reduction of fatigue striation spacing and the monitoring of fatigue crack growth corroborate that the LSP decreases the fatigue crack growth rate in both sample geometries. However, the propagation direction of fatigue crack growth in fillet samples decreases the crack incubation time. This material behavior is related to the residual stress distribution and the anisotropy of this steel. It is evident that the sample geometry is an important factor to the residual stress distribution and the fatigue life of 2205 DSS.

Data Availability

The experimental data used to support the findings of this study are included within the article.

Conflicts of Interest

The authors declare that there are no conflicts of interest regarding the publication of this paper.

Acknowledgments

The authors thank the University of Colima, CIDESI, University of Guadalajara, and CONACYT (Mexico) for their support in the realization of this work.

References

[1] M. Kattoura, S. R. Mannava, D. Qian, and V. K. Vasudevan, "Effect of laser shock peening on residual stress, microstructure and fatigue behavior of ATI 718Plus alloy," *International Journal of Fatigue*, vol. 102, pp. 121–134, 2017.

[2] C. Rubiogonzalez, J. L. Ocana, G. Gomezrosas et al., "Effect of laser shock processing on fatigue crack growth and fracture toughness of 6061-T6 aluminum alloy," *Materials Science and Engineering A*, vol. 386, no. 1-2, pp. 291–295, 2004.

[3] C. Rubio-González, C. Felix-Martinez, G. Gomez-Rosas, J. L. Ocaña, M. Morales, and J. A. Porro, "Effect of laser shock processing on fatigue crack growth of duplex stainless steel," *Materials Science and Engineering: A*, vol. 528, no. 3, pp. 914–919, 2011.

[4] S. Bhamare, G. Ramakrishnan, S. R. Mannava, K. Langer, V. K. Vasudevan, and D. Qian, "Simulation-based optimization of laser shock peening process for improved bending fatigue life of Ti-6Al-2Sn-4Zr-2Mo alloy," *Surface and Coatings Technology*, vol. 232, pp. 464–474, 2013.

[5] C. Correa, L. Ruiz De Lara, M. Díaz, J. A. Porro, A. García-Beltrán, and J. L. Ocaña, "Influence of pulse sequence and edge material effect on fatigue life of Al2024-T351 specimens treated by laser shock processing," *International Journal of Fatigue*, vol. 70, pp. 196–204, 2015.

[6] C. A. Vázquez Jiménez, G. Gómez Rosas, C. Rubio González, V. Granados Alejo, and S. Hereñú, "Effect of laser shock processing on fatigue life of 2205 duplex stainless steel notched specimens," *Optics & Laser Technology*, vol. 97, pp. 308–315, 2017.

[7] C. Correa, L. Ruiz De Lara, M. Díaz, A. Gil-Santos, J. A. Porro, and J. L. Ocaña, "Effect of advancing direction on fatigue life of 316L stainless steel specimens treated by double-sided laser shock peening," *International Journal of Fatigue*, vol. 79, pp. 1–9, 2015.

[8] J. Sheng, S. Huang, J. Z. Zhou, J. Z. Lu, S. Q. Xu, and H. F. Zhang, "Effect of laser peening with different energies on fatigue fracture evolution of 6061-T6 aluminum alloy," *Optics & Laser Technology*, vol. 77, pp. 169–176, 2016.

[9] S. Huang, J. Z. Zhou, J. Sheng et al., "Effects of laser energy on fatigue crack growth properties of 6061-T6 aluminum alloy subjected to multiple laser peening," *Engineering Fracture Mechanics*, vol. 99, pp. 87–100, 2013.

[10] S. Huang, J. Sheng, J. Z. Zhou et al., "On the influence of laser peening with different coverage areas on fatigue response and fracture behavior of Ti-6Al-4V alloy," *Engineering Fracture Mechanics*, vol. 147, pp. 72–82, 2015.

[11] S. Huang, J. Z. Zhou, J. Sheng et al., "Effects of laser peening with different coverage areas on fatigue crack growth properties of 6061-T6 aluminum alloy," *International Journal of Fatigue*, vol. 47, pp. 292–299, 2013.

[12] M. Kattoura, S. R. Mannava, D. Qian, and V. K. Vasudevan, "Effect of laser shock peening on elevated temperature residual stress, microstructure and fatigue behavior of ATI 718Plus alloy," *International Journal of Fatigue*, vol. 104, pp. 366–378, 2017.

[13] J. T. Wang, Y. K. Zhang, J. F. Chen et al., "Effect of laser shock peening on the high-temperature fatigue performance of 7075 aluminum alloy," *Materials Science and Engineering: A*, vol. 704, pp. 459–468, 2017.

[14] V. Granados-alejo, C. Rubio-gonzalez, and Y. Parra-torres, "Influence of laser peening on fatigue crack initiation of notched aluminum plates," *Structural Engineering and Mechanics*, vol. 6, pp. 739–748, 2017.

[15] S. Prabhakaran and S. Kalainathan, "Compound technology of manufacturing and multiple laser peening on microstructure and fatigue life of dual-phase spring steel," *Materials Science and Engineering: A*, vol. 674, pp. 634–645, 2016.

[16] C. Rubio-gonzalez, G. Gomez-Rosas, R. Ruiz, M. Nait, and A. Amrouche, "Effect of laser shock peening and cold expansion on fatigue performance of open hole samples," *Structural Engineering and Mechanics*, vol. 53, no. 5, pp. 867–880, 2015.

[17] L. Spadaro, G. Gomez-Rosas, C. Rubio-González, R. Bolmaro, A. Chavez-Chavez, and S. Hereñú, "Fatigue behavior of superferritic stainless steel laser shock treated without protective coating," *Optics & Laser Technology*, vol. 93, pp. 208–215, 2017.

[18] Z. Bergant, U. Trdan, and J. Grum, "Effects of laser shock processing on high cycle fatigue crack growth rate and fracture toughness of aluminium alloy 6082-T651," *International Journal of Fatigue*, vol. 87, pp. 444–455, 2016.

[19] V. Granados-Alejo, C. Rubio-González, C. A. Vázquez-Jiménez, J. A. Banderas, and G. Gómez-Rosas, "Influence of specimen thickness on the fatigue behavior of notched steel plates subjected to laser shock peening," *Optics & Laser Technology*, vol. 101, pp. 531–544, 2018.

[20] M. Achintha, D. Nowell, D. Fufari, E. E. Sackett, and M. R. Bache, "Fatigue behaviour of geometric features subjected to laser shock peening: experiments and modelling," *International Journal of Fatigue*, vol. 62, pp. 171–179, 2014.

[21] G. Ivetic, I. Meneghin, E. Troiani et al., "Fatigue in laser shock peened open-hole thin aluminium specimens," *Materials Science and Engineering: A*, vol. 534, pp. 573–579, 2012.

[22] X. Q. Zhang, L. S. Chen, S. Z. Li et al., "Investigation of the fatigue life of pre- and post-drilling hole in dog-bone specimen subjected to laser shot peening," *Materials & Design*, vol. 88, pp. 106–114, 2015.

[23] N. Hfaiedh, P. Peyre, H. Song, I. Popa, V. Ji, and V. Vignal, "Finite element analysis of laser shock peening of 2050-T8 aluminum alloy," *International Journal of Fatigue*, vol. 70, pp. 480–489, 2015.

[24] E. A. Larson, X. Ren, S. Adu-Gyamfi, H. Zhang, and Y. Ren, "Effects of scanning path gradient on the residual stress distribution and fatigue life of AA2024-T351 aluminium alloy induced by LSP," *Results in Physics*, vol. 13, Article ID 102123, 2019.

[25] S. Adu-Gyamfi, X. D. Ren, E. A. Larson, Y. Ren, and Z. Tong, "The effects of laser shock peening scanning patterns on residual stress distribution and fatigue life of AA2024 aluminium alloy," *Optics & Laser Technology*, vol. 108, pp. 177–185, 2018.

[26] K. Y. Luo, Y. F. Yin, C. Y. Wang et al., "Effects of laser shock peening with different coverage layers on fatigue behaviour and fractural morphology of Fe-Cr alloy in NaCl solution," *Journal of Alloys and Compounds*, vol. 773, pp. 168–179, 2019.

[27] Y. Jiang, X. Li, W. Jiang et al., "Thickness effect in laser shock processing for test specimens with a small hole under smaller laser power density," *Optics & Laser Technology*, vol. 114, pp. 127–134, 2019.

[28] A. Mateo, L. Llanes, N. Akdut, J. Stolarz, and M. Anglada, "Anisotropy effects on the fatigue behaviour of rolled duplex stainless steels," *International Journal of Fatigue*, vol. 25, no. 6, pp. 481–488, 2003.

[29] C. A. Vázquez Jiménez, G. Gómez Rosas, C. Rubio González, V. Granados Alejo, and S. Hereñú, "Effect of laser shock processing on fatigue life of 2205 duplex stainless steel notched specimens," *Optics & Laser Technology*, vol. 97, 2017.

[30] J. C. De Lacerda, L. C. Cândido, and L. B. Godefroid, "Effect of volume fraction of phases and precipitates on the mechanical behavior of UNS S31803 duplex stainless steel," *International Journal of Fatigue*, vol. 74, pp. 81–87, 2015.

[31] G. Fargas, N. Akdut, M. Anglada, and A. Mateo, "Reduction of anisotropy in cold-rolled duplex stainless steel sheets by using sigma phase transformation," *Metallurgical and Materials Transactions A*, vol. 42, no. 11, pp. 3472–3483, 2011.

[32] X. Q. Zhang, H. Li, X. L. Yu et al., "Investigation on effect of laser shock processing on fatigue crack initiation and its growth in aluminum alloy plate," *Materials & Design (1980–2015)*, vol. 65, pp. 425–431, 2015.

[33] C. A. Vázquez Jiménez, R. Strubbia, G. Gómez Rosas, C. Rubio González, and S. Hereñú, "Fatigue life rationalization of laser shock peened SAF 2205 with different swept direction," *Optics & Laser Technology*, vol. 111, pp. 789–796, 2019.